

# Study on high-efficiency cutting of high-thickness workpiece with stranded wire electrode in high-speed wire electrical discharge machining

Yichao Ji<sup>1</sup> · Zhidong Liu<sup>1</sup> · Cong Deng<sup>1</sup> · Laijiu Fang<sup>1</sup> · Mingbo Qiu<sup>1</sup>

Received: 28 April 2018 / Accepted: 17 September 2018 / Published online: 1 October 2018

© Springer-Verlag London Ltd., part of Springer Nature 2018

## Abstract

To further improve the technological indexes of high-speed wire electrical discharge machining (HS-WEDM) under conditions of high energy and high thickness while also solving the problem of an absent liquid medium and unsteady processing in the inter-electrode gap, a new type of stranded wire electrode used in HS-WEDM was designed to enhance the flow of the liquid medium and debris removal during the machining process. First, a simulation model of the inter-electrode gap flow field is established; the simulation analysis indicates that the capacity of carrying liquid medium with a stranded wire electrode is approximately 65% higher than with a normal wire electrode at a high workpiece thickness of 400 mm. Next, the special discharge characteristic of stranded wire electrode is summarized from the two aspects of effective discharge area and high-thickness workpiece. Third, a comparative experiment on cutting a high-thickness workpiece at high energy demonstrates a greater threshold of stable cutting speed (over 250 mm<sup>2</sup>/min) and stable material removal rate (142 mm<sup>3</sup>/min) at an average cutting current of 18 A with a stranded wire electrode, whereas the maximum cutting speed (155 mm<sup>2</sup>/min) at an average cutting current of 8 A with a normal wire electrode. Experiments prove that using a stranded wire electrode can significantly increase cutting speed and improve processing stability in the electrode gap under high-energy and high-thickness conditions.

**Keywords** High-speed reciprocating traveling · WEDM · Stranded wire electrode · High thickness · High cutting speed

## 1 Introduction

High-speed wire electrical discharge machining (HS-WEDM) has been widely used in precision molds, aviation, aerospace, military, automobile, and other machinery manufacturing industry applications and has become an indispensable modern manufacturing process [1–4]. At present, the highest cutting speed of low-speed wire electrical discharge machining has been improved to 500 mm<sup>2</sup>/min under lower-thickness condition [5], but it significantly reduced and the probability of a broken wire increased greatly in the case of high-thickness workpieces (over 200 mm). The stable cutting speed of the Chinese self-developed HS-WEDM is generally approximately 150 mm<sup>2</sup>/min. The discharge state becomes extremely

unstable, and the cutting efficiency also drops sharply as the thickness of the workpiece increases [6]. The liquid medium in the electrode gap is insufficient for efficient cooling, cleaning, and removal of debris from the machining gap [7]. Therefore, it is essential to enhance the flow of the liquid medium to improve the cutting speed of high-thickness workpieces. This paper aims to design a new type of stranded wire electrode to increase high-thickness cutting speed by enhancing the flow of the liquid medium and debris removal during the machining process.

## 2 Experimental conditions

A stranded wire electrode was constructed of two normal wire electrodes with a diameter of Φ0.18 mm and twisted at 360 degrees per 10 mm (strand distance), unlike normal wire electrodes. Thus, it was necessary to choose an equivalent wire electrode to compare the cutting performance of the two types of wire electrodes. According to the equivalent relation of the cross-sectional area of the wire electrode, the relationship

✉ Zhidong Liu  
m18851177635@163.com

<sup>1</sup> College of Mechanical and Electrical Engineering, Nanjing University of Aeronautics and Astronautics, Nanjing 210016, China

between the diameter of the single wire electrode of the stranded wire electrode ( $d$ ) and that of the equivalent wire electrode ( $D$ ) can be calculated as follows:

$$2 \times \pi \times \left(\frac{d}{2}\right)^2 = \pi \times \left(\frac{D}{2}\right)^2 \quad (1)$$

Therefore,

$$D = \sqrt{2}d \quad (2)$$

By substituting  $d = 0.18$  mm into Eq. (2), we can determine that  $D \approx 0.25$  mm. The stranded wire electrode picture and the equivalent relationship of the cross-sectional area of the wire electrode are shown in Fig. 1.

The experiment was conducted using the HF500A HS-WEDM (see Fig. 2).

### 3 Simulation analysis of inter-electrode gap flow field with stranded wire electrode

#### 3.1 Model and boundary conditions of the stranded wire electrode

To research the liquid medium carrying capacity of the stranded wire electrode, a model of the inter-electrode gap flow field was established to analyze and simulate the flow field of the stranded wire electrode and normal wire electrode, respectively, using ANSYS fluid simulation software under the condition of a workpiece thickness of 400 mm. Because the shear flow rate was three orders of magnitude greater than the differential pressure flow rate in the inter-electrode gap flow field [8], the effect of shear flow on the liquid medium carrying

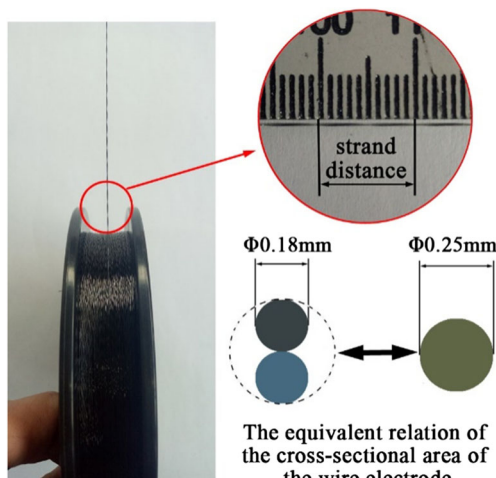


**Fig. 1** Photograph of stranded wire electrode and equivalent relationship of cross-sectional area of wire electrode

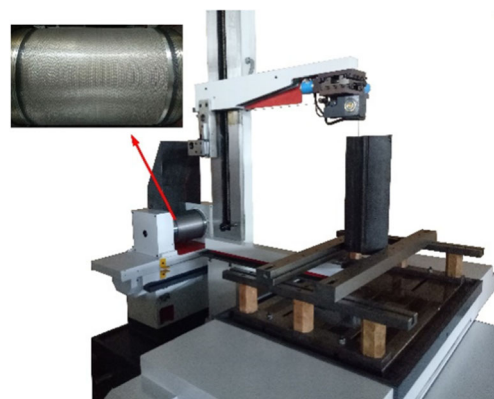


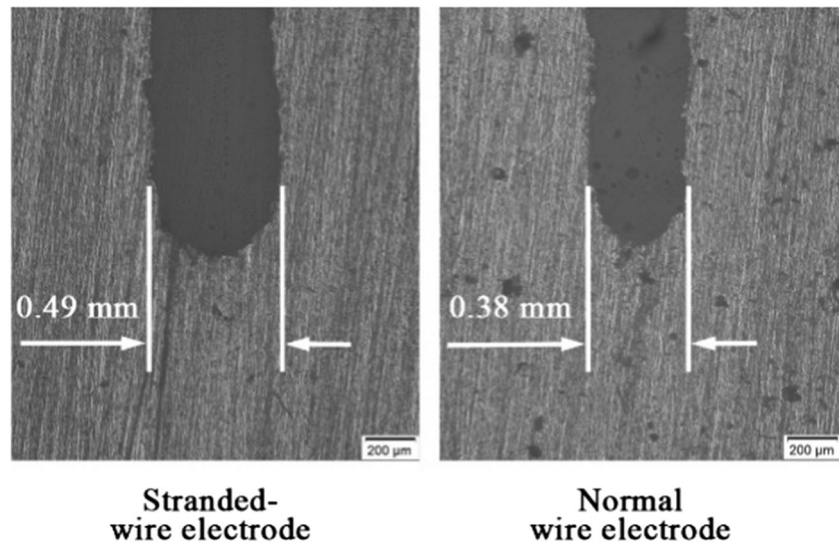
**Fig. 2** Photograph of experimental equipment

capacity of the wire electrode was simulated and analyzed in this paper. The machined slot of the stranded wire electrode and the normal wire electrode is shown in Fig. 3; therefore, to improve analysis, it is necessary to establish a cylindrical fluid domain which is the same width as the machined slot,  $Ls1 = 0.49$  mm,  $Ls2 = 0.38$  mm (i.e., simulation model of the flow region near the workpiece side), called the static watershed. We also need a cylindrical fluid domain slightly smaller than the diameter of static watershed,  $Ld1 = 0.47$  mm,  $Ld2 = 0.36$  mm (i.e., simulation model of the flow region near the electrode wire side) called the dynamic watershed. The upper and lower end faces and side faces between the dynamic watershed and static watershed were defined as the interface 1, interface 2, and interface 3, and the velocity of the dynamic watershed was set at 12 m/s the same speed as the wire electrode. The wire electrode surface was defined as a moving wall and the outer surface of static watershed was defined as an outer wall, simulated using a moving reference frame (MRF) dynamic mesh model, the model of the inter-electrode gap flow field is shown in Fig. 4. The gravity acceleration was  $-9.81$  m/s $^2$ , liquid medium density was  $1.0 \times 10^3$  kg/m $^3$ , and dynamic viscosity coefficient was  $1.14 \times 10^{-3}$  Pa·s.

#### 3.2 Simulation result analysis

Because of the influence of gravity, the cooling, cleaning, and debris removal in the machining process were all asymmetrical [9], and the capacity of carrying liquid medium changed with the running direction of the wire electrode. Therefore, this study simulated the upward and downward movement of the wire electrode; the flow speed vector of the fluid medium in different running directions is shown in Figs. 5 and 6. The discharge channel indicated that the surface of the stranded wire electrode was distributed in a bright-colored spiral, whereas the surface of the normal wire electrode was denoted by a flat, darker color, suggesting that the spiral flow velocity of the fluid medium in the flow field of the stranded wire electrode was higher than the linear flow velocity of the fluid

**Fig. 3** Machined slot of the stranded wire electrode and the normal wire electrode



medium in the flow field of the normal wire electrode. Regardless of the direction of the wire electrode, the outlet of the dynamic watershed demonstrated that the outlet color of the stranded wire electrode was brighter than that of the normal wire electrode, indicating that the flow speed of the dynamic watershed in the stranded wire electrode field was higher. According to the results of the simulation calculation, the flow rate of the cross-section of the stranded wire electrode was 1.65 times that of the normal electrode in the outlet of the dynamic watershed. The above analysis shows that the stranded wire electrode has better liquid medium carrying capacity than the normal wire electrode in HS-WEDM.

#### 4 Discharge characteristics of stranded wire electrode

##### 4.1 Analysis of effective discharge area of stranded wire electrode

In the HS-WEDM process, given the microscopic uneven surface of the workpiece and wire electrode, the point of maximum field strength must be the closest point between the workpiece and the wire electrode when every pulse discharge occurs [10], where the discharge channel is also most easily formed through the breakdown of the fluid medium.

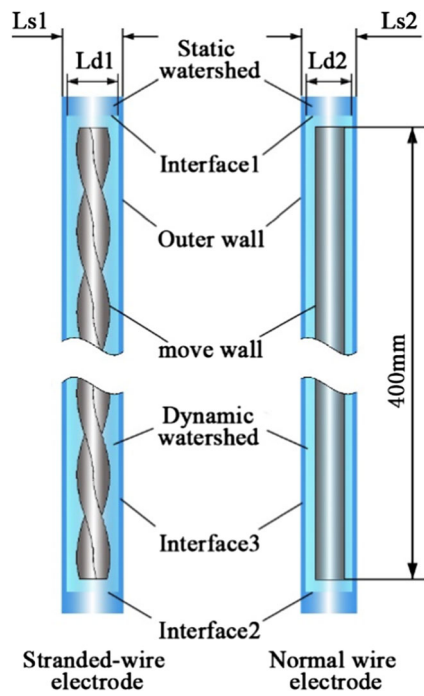


**Fig. 4** Simulation model of inter-electrode gap flow field

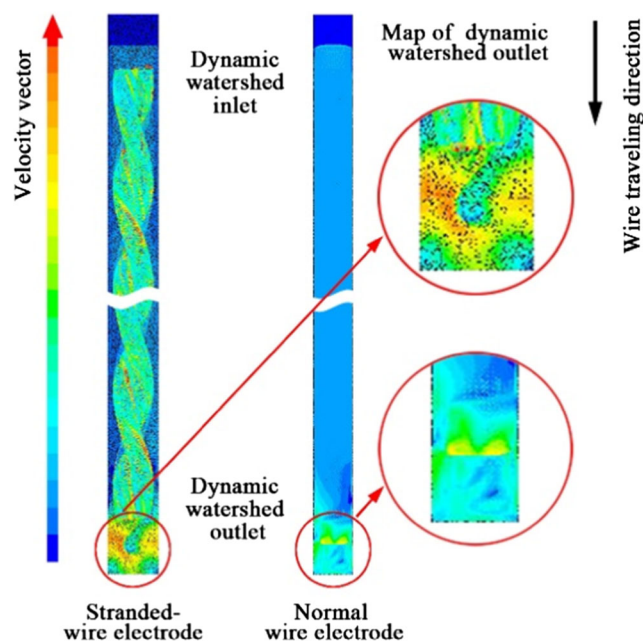


**Fig. 5** Flow velocity vector diagram of fluid medium when wire electrode runs down

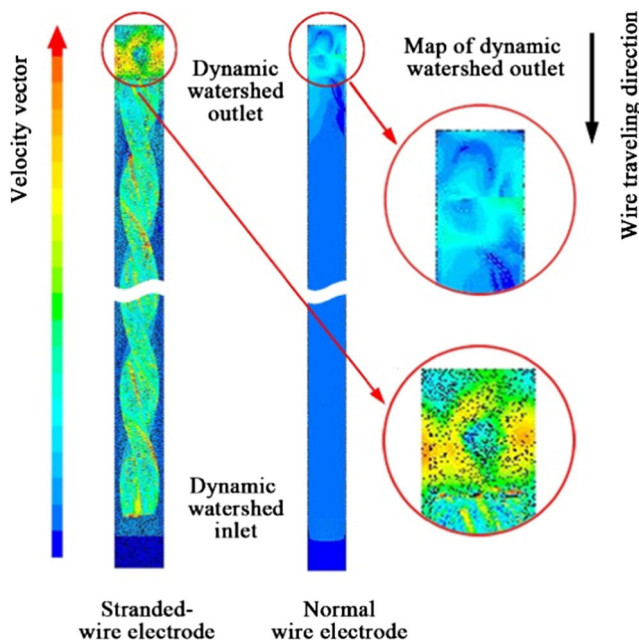
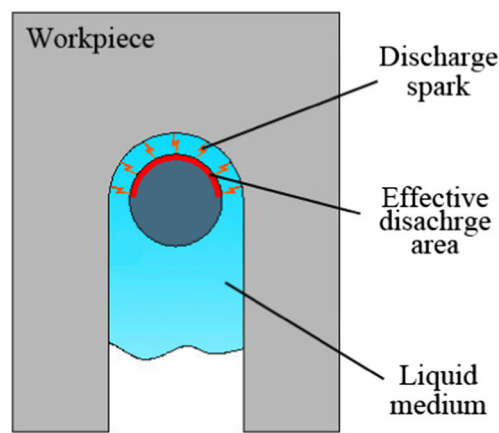


**Fig. 6** Flow velocity vector diagram of fluid medium when wire electrode runs up

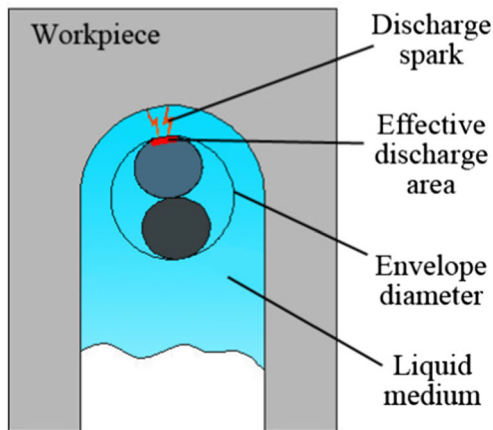
Therefore, to improve analysis, a cross-section discharge model of the stranded wire electrode and normal wire electrode was established and is presented in Fig. 7; it incorporates the major factors affecting the electrode gap. The theoretical assumptions of this model are as follows:

1. The normal wire electrode is a uniform cylinder, its surface is smooth, and the position of the wire electrode in the slit is straight. The surface of the stranded wire electrode is also uniform and smooth, and the stranded wire electrode is stranded tightly and uniformly.
2. The arc section of the cutting slit is a regular arc, the cutting surface is smooth, and the axis of the wire electrode is the same as the slit arc.
3. No impurities or bubbles appear in the inter-electrode dielectric fluid, and the inter-electrode gap is filled evenly with dielectric fluid.

The cross-section discharge model of the normal wire electrode is shown in Fig. 7a. The distance was found to be consistent between the semicircular outer surface of the normal wire electrode and the workpiece in processing direction. When a voltage pulse occurred, the normal wire electrode participated in the pulse discharge on the semicircular surface in the processing direction, where the effective discharge surface was the semicircular surface of the normal wire electrode. The cross-section discharge model of the stranded wire electrode is shown in Fig. 7b. Although the envelope outer diameter of the stranded wire electrode was larger than that of the normal wire electrode, only a small part of its outer surface



(a) Normal wire electrode



(b) Stranded-wire electrode

**Fig. 7** Cross-section discharge model of stranded wire electrode and normal wire electrode

was close to the workpiece in the processing direction in the discharge channel because of its spiral structure. When a voltage pulse occurred, the stranded wire electrode only participated in the pulse discharge on the convex outer surface in the processing direction, where the effective discharge surface was the outer surface coinciding with the envelope outer diameter of the stranded wire electrode. The effective discharge area of the stranded wire electrode was therefore far less than that of the normal wire electrode in the processing direction.

#### 4.2 Analysis of discharge characteristics of stranded wire electrode in high-thickness workpiece

##### 4.2.1 Analysis of the discharge characteristic of stranded wire electrode in a thin-layer of high-thickness workpiece

To explore the microcosmic discharge characteristic of a stranded wire electrode in a high-thickness workpiece, a thin-layer of a high-thickness workpiece was analyzed

separately under the assumption that the material removal rate of the workpiece was consistent with the feed speed of the stranded wire electrode. The discharge model of the stranded wire electrode close to the thin-layer is shown in Fig. 8. The machined state of four kinds of stranded wire electrodes (A, B, C, and D) represent the four different positions that the stranded wire electrode went through the length of a stranded distance of the thin-layer. Due to the special spiral shape of the stranded wire electrode, only the position of the convex outer surface in the machining direction formed normal discharge with the thin-layer, with the discharge length on the stranded wire electrode defined as the effective discharge length. The effective discharge length of the stranded wire electrode in the processing direction was located only in the thin-layer body in the A and C positions, and normal machining discharge was formed with the workpiece. While continuous voltage pulse was applied between the stranded wire electrode and the workpiece in the B and D positions, the stranded wire electrode had no convex outer surface in the thin-layer body, leading to no normal machining discharge between the wire electrode and the workpiece.

From the above analysis, the characteristic close to the thin-layer of the stranded wire electrode through the length of a stranded distance of the thin-layer is as follows:

$$T_A = T_C = \frac{l}{\nu} \quad (3)$$

$$T_B = T_D = \frac{d-2l}{2\nu} \quad (4)$$

where  $T_A$ ,  $T_B$ ,  $T_C$ , and  $T_D$  denote the time at which the A, B, C, and D stranded wire electrodes pass through thin layer (s), respectively;  $d$  denotes the stranded distance of the stranded wire electrode (mm);  $l$  denotes the effective discharge length

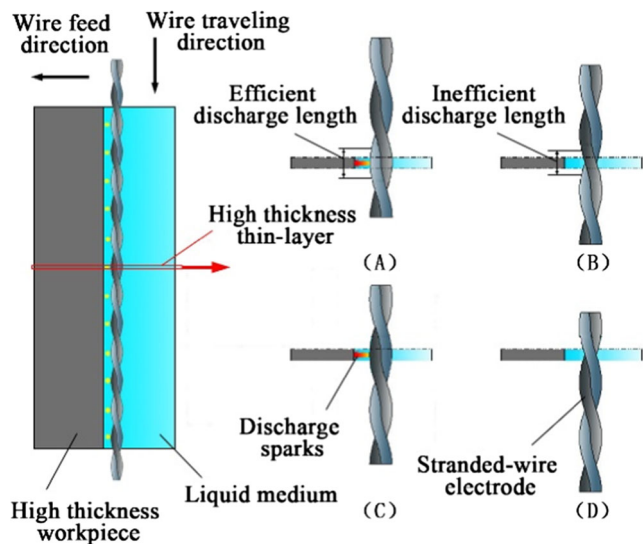


**Fig. 8** Discharge model of stranded wire electrode close to the thin-layer

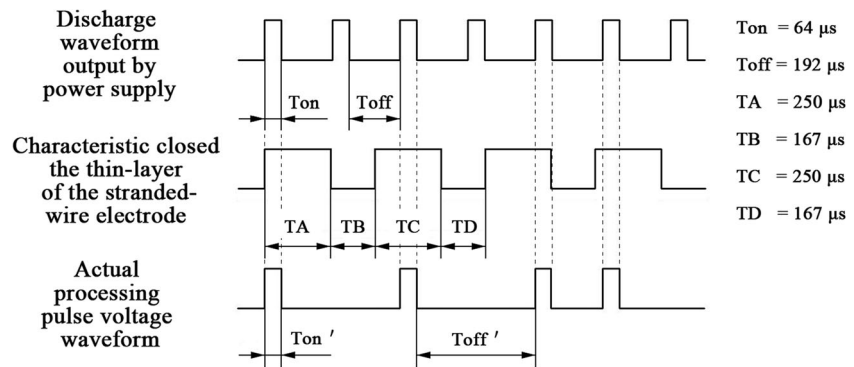
on the stranded wire electrode ( $l < \frac{1}{2}d$ ) (mm); and  $\nu$  denotes the speed of the stranded wire electrode (mm/s).

In the HS-WEDM process, the speed of the wire electrode is 12 m/s and  $T_A$ ,  $T_B$ ,  $T_C$ , and  $T_D$  are all  $\mu$ s degree. Thus, the characteristic of the stranded wire electrode closed thin-layer can be considered a pulse waveform with a pulse width of  $T_A(T_C)$  and a pulse interval of  $T_B(T_D)$ . The voltage pulse produced by the power supply in HS-WEDM is a set of discharge waveforms with a pulse interval, and the actual processing voltage pulse waveform can be obtained by superposing the characteristic of the stranded wire electrode closed thin-layer under a hypothetical condition and the discharge waveform output by the power supply. Because the actual processing pulse waveform is influenced by multiple factors, a simple analysis of the discharge waveform was drawn to illustrate the discharge characteristic of the stranded wire electrode in a thin-layer of a high-thickness workpiece. In this case, the pulse width of the power supply was 64  $\mu$ s, the duty ratio was 4, and the effective discharge length on the stranded wire electrode was 3 mm; the schematic diagram of the discharge waveform in the actual machining of the stranded wire electrode is shown in Fig. 9. The actual processing pulse voltage waveform was no longer a regular pulse waveform in a thin-layer of the high-thickness workpiece; rather, it was forced to join many undetermined time pulse intervals under superposition of the characteristic of the stranded wire electrode closed thin-layer and the discharge waveform output by the power supply. Thus, the effective pulse width shortened from  $T_{on}$  to  $T_{on}'$ , and the effective pulse interval increased from  $T_{off}$  to  $T_{off}'$ .

#### 4.2.2 Analysis of discharge characteristic of stranded wire electrode in high-thickness workpiece

Processing difficulty was found to increase with an increase in workpiece thickness when machined using HS-WEDM [11]. The main problem is twofold. First, due to the low liquid medium carrying capacity of the normal wire electrode in a high-thickness workpiece and insufficient supply of fluid medium in the inter-electrode gap, the cooling, cleaning, and debris removal were each affected, exacerbating the inter-electrode discharge state and increasing the difficulty of cutting the high-thickness workpiece. Second, according to analysis of the effective discharge area of the wire electrode, the effective discharge surface of the normal wire electrode was a semicircular surface in the machining direction, and the surface was uneven; as such, the discharge of the normal wire electrode in the entire discharge channel occurred randomly (i.e., the discharge position of the normal wire electrode in the machining process was random), which led easily to multiple discharges in the same position on the high-thickness workpiece in a short time. Debris accumulates easily under such conditions, resulting in a bridging phenomenon and burning

**Fig. 9** Schematic diagram of discharge waveform in actual machining of stranded wire electrode



of the wire electrode, thereby reducing the utilization rate of effective discharge pulses and increasing the instability of electrical discharge machining. The discharge characteristic and probability of effective discharge pulse of the normal wire electrode are shown in Fig. 10.

In the process of machining a high-thickness workpiece, the discharge characteristic of the new stranded wire electrode can be analyzed based on physical structure and micro-discharge; the discharge characteristic and probability of effective discharge pulse of the stranded wire electrode are shown in Fig. 11. First, the stranded wire electrode could carry more fluid medium into the inter-electrode gap and improve cleaning, debris removal, and deionization to ensure the stability of the discharge state in the machining gap, owing to a spiral groove structure shape. It could also hold more debris in the grooves and expel it in time to prevent debris from clogging the discharge channel. Second, as depicted in Fig. 11, a

regular discharge surface existed between the stranded wire electrode and the workpiece in the processing direction, which was spirally distributed in the discharge channel. With a fixed discharge position in the discharge channel of a high-thickness workpiece, the spiral-distributed discharge surface actually increased the discharge interval of each position. As mentioned above, numerous indeterminate pulse intervals were added to the thin layer of the high-thickness workpiece, benefiting debris removal and deionization. In the discharge channel of a high-thickness workpiece, each discharge position of the stranded wire electrode was forcibly separated for a period of time before the second discharge, effectively avoiding arcing and burning of the broken wire electrode due to the phenomenon of concentrated discharge within a short period of time at the same position. This discharge characteristic further improves cleaning, debris removal, and deionization under conditions of high energy and high thickness.

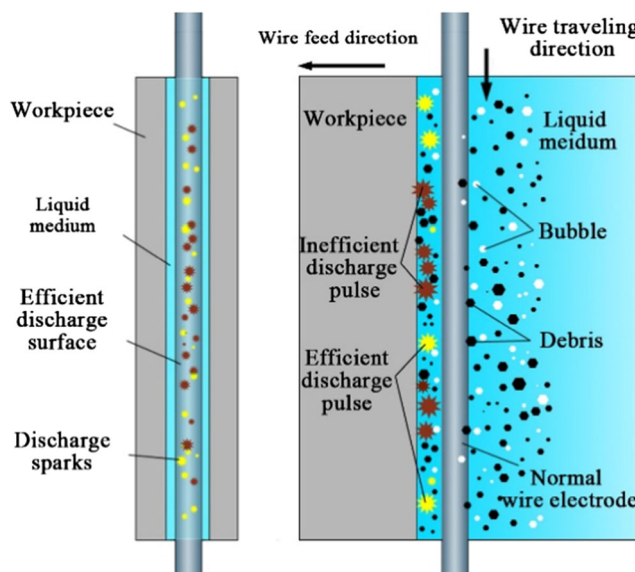


**Fig. 10** Discharge characteristic and probability of effective discharge pulse of normal wire electrode

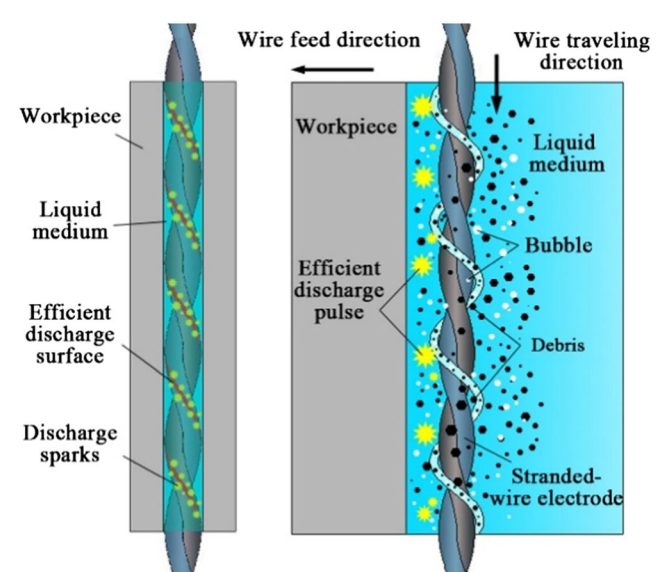


**Fig. 11** Discharge characteristic and probability of effective discharge pulse of stranded-wire electrode

**Table 1** Parameters of material and wire electrode

Item	Parameter
Stranded wire electrode	Single diameter = 0.18 mm, envelope outer diameter = 0.36 mm, stranded distance = 10 mm, length = 200 m
Normal wire electrode	Diameter = 0.25 mm, length = 200 m
Material	45 carbon steel, thickness = 400 mm
Wire speed	12 m/s

Therefore, regular discharge of the stranded wire electrode will greatly improve the discharge state in the machining gap, enhance processing stability, and improve the probability of effective discharge pulses.

## 5 Probability analysis of effective discharge pulse and test verification of the normal wire electrode and stranded wire electrode

In this experiment, a working fluid with JR1A-to-water ratio (1:10) was used to verify the discharge characteristics of the stranded wire electrode and normal wire electrode in the processing of high-thickness workpieces. The probability of effective discharge pulse in two kinds of wire electrode was analyzed indirectly [12]. The parameters of the material and wire electrode are listed in Table 1; the machining parameters of the pulse power supply are listed in Table 2.

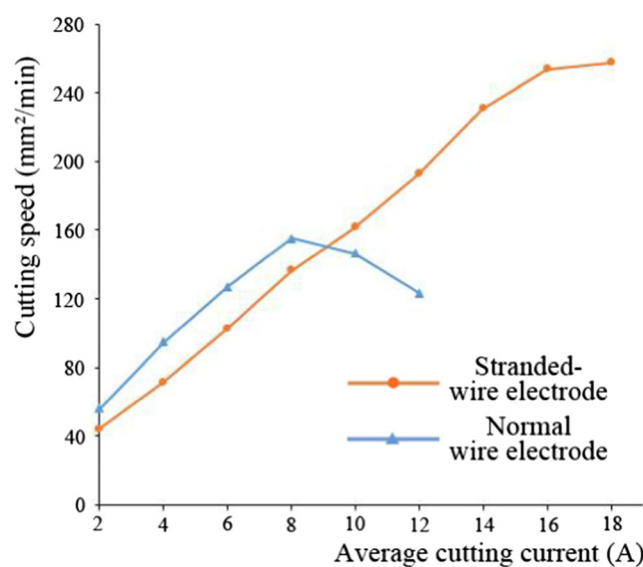
### 5.1 Analysis of cutting speed and material removal rate under processing conditions of two kinds of wire electrode

Figure 12 illustrates the relationship between the cutting speed and average cutting current under the processing conditions of two kinds of wire electrodes. Both curves demonstrate a different trend with an increase in the average cutting current.

**Table 2** Parameters of pulse power supply

Pulse-on time (μs)	Duty ratio	Number of MOS tube	Average cutting current (A)
64	1:8	2	2
64	1:9	5	4
64	1:8	7	6
64	1:7	9	8
64	1:6	10	10
64	1:5	10	12
64	1:4	10	14
64	1:4	12	16
64	1:4	14	18

First, when the average cutting current is less than 8 A, a proportional rise occurs in the cutting speed of two kinds of wire electrode with increasing average cutting current, during which the cutting speed of the normal wire electrode was even higher than that of the stranded wire electrode, and the normal wire electrode reached a maximum cutting speed of 155 mm<sup>2</sup>/min on an average cutting current of 8 A, suggesting that the discharge state of the two kinds of wire electrodes was still normal. When the average cutting current increased from 8 A to 16 A, the cutting speed of the normal wire electrode exhibited a downward trend, and adverse discharge (especially short circuiting) occurred frequently on an average cutting current of 12 A, indicating that the inter-electrode discharge state of the normal wire electrode began to deteriorate, and the process became extremely unstable and unsuitable for machining when the average cutting current was above 12 A. The cutting speed of stranded wire electrode continued to rise similar to the original pattern and exceeded the normal wire electrode on an average cutting current of 10 A, indicating that the stranded wire electrode manages to maintain a good inter-electrode discharge state. When the average cutting current increased from 16 A to 18 A, the cutting speed began to increase slowly and reached a maximum of 257 mm<sup>2</sup>/min

**Fig. 12** Relationship between cutting speed and average cutting current under processing conditions of two kinds of wire electrodes

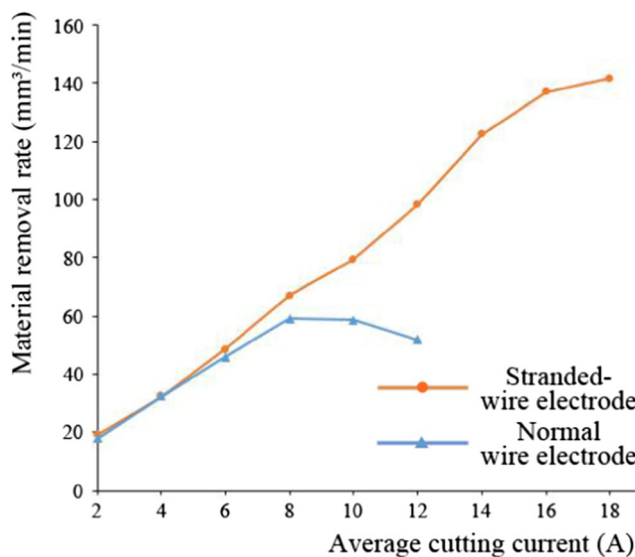


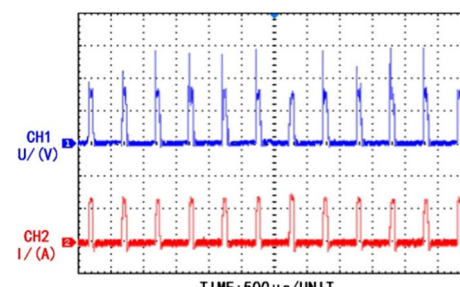
**Fig. 13** Relationship between material removal rate and average cutting current under processing conditions of two kinds of wire electrodes

on the current at 18 A, suggesting that the discharge state began to deteriorate but could still support normal discharge machining.

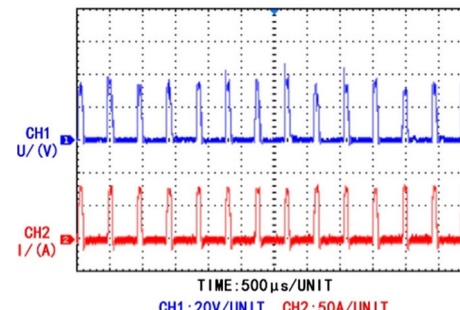
Figure 13 illustrates the relationship between the material removal rate and average cutting current under the processing conditions of two kinds of wire electrodes. In the region where the average cutting current varied from 2 A to 18 A, the material removal rate of the stranded wire electrode was consistently higher than that of the normal wire electrode, and the material removal rate difference for the two kinds of wire electrodes increased gradually with an increase in the cutting current; this finding suggests that the stranded wire electrode can maintain better inert-electrode discharge state than the normal wire electrode to achieve high-efficiency cutting under conditions of high energy and high thickness [13].

## 5.2 Analysis of inter-electrode discharge state under processing conditions of two kinds of wire electrode

In the HS-WEDM process, discharge waveforms can monitor the electrode gap condition and reflect the stability of the machining process [14–16]. Figure 14a, b depicts the waveforms of the continuous discharge current and voltage during the experiment conducted at the same energy (average cutting current of 8 A and 10 A, pulse-on time of 64 μs) under processing conditions of two kinds of wire electrodes. Most waveforms of the discharge voltage exhibited a breakdown time delay when the average current was 8 A, whereas most waveforms showed no such delay at an average current of 10 A under the normal wire electrode processing conditions. Nearly all waveforms demonstrated a time delay with an

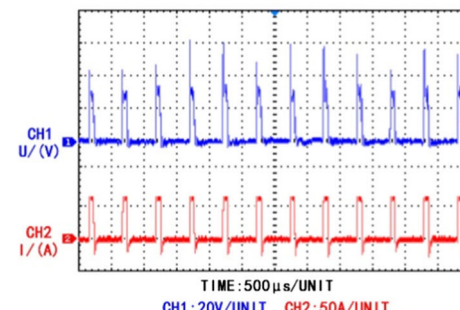


Average cutting current = 8 A

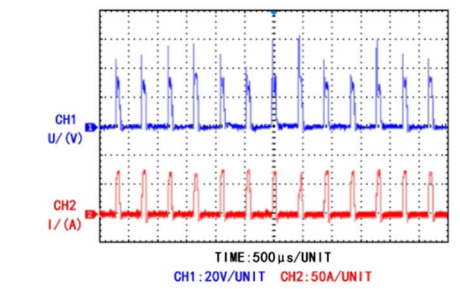


Average cutting current = 10 A

(a) Waveforms of continuous discharge under processing conditions of normal wire electrode



Average cutting current = 8 A

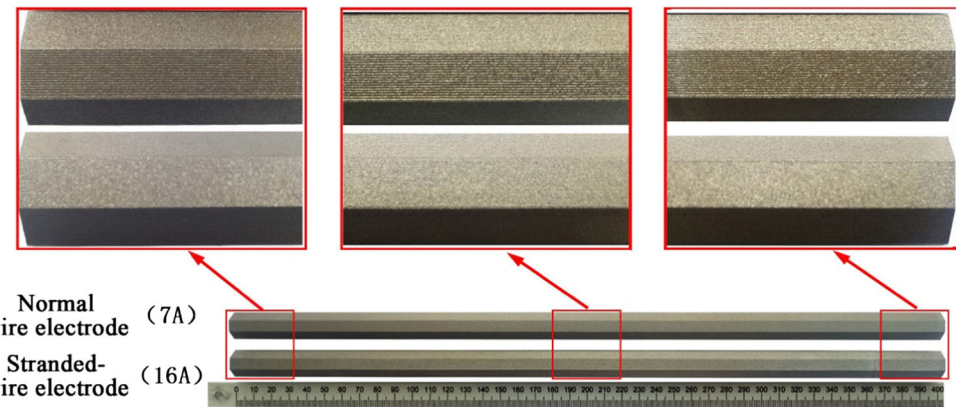


Average cutting current = 10 A

(b) Waveforms of continuous discharge under processing conditions of stranded-wire electrode

**Fig. 14** Waveforms of continuous discharge under different wire electrodes (current = 8 A and 10 A; pulse-on time = 64 μs)

**Fig. 15** Cutting surface under processing conditions of two kinds of wire electrodes



average current of 8 A and 10 A under processing conditions of the stranded wire electrode. The breakdown time delay reflects the condition of the inter-electrode working medium: if the voltage waveform experienced a breakdown time delay, then the machining gap filled with dielectric fluid, which required time to ionize and form a plasma channel. On the other hand, when the waveform experienced no discharge delay, the physical state of the liquid medium deteriorated, and the utilization rate of the discharge pulse declined substantially.

### 5.3 Analysis of surface evenness of workpiece under processing conditions of two kinds of wire electrode

To further study the influence of the discharge state under different wire electrodes on machined surface, workpiece photographs with a normal wire electrode at an average cutting current of 7 A and those with a stranded wire electrode at an average cutting current of 16 A were compared. The normal wire electrode could not be cut for long when the average cutting current was more than 8 A. The shape of the workpiece had an eight-sided shape at a side length of 6 mm, and the workpiece thickness was 400 mm as shown in Fig. 15. The surface evenness of the two kinds of workpieces under different processing conditions was not substantially different; the cutting surfaces were each relatively smooth and bright with lighter stripes and with no black sinter, indicating that the cutting stability of the stranded wire electrode at an average cutting current of 16 A was similar to that of the normal wire electrode at an average cutting current of 7 A.

According to analysis of the cutting speed, material removal rate, discharge waveforms in the electrode gap, and surface evenness of the workpiece, the cutting speed and surface evenness of the stranded wire electrode appeared better than that of the normal wire electrode under conditions of high energy and high thickness. This finding substantiates the superiority of the stranded wire electrode. In short, a stranded wire electrode with a high liquid carrying capacity and debris removal can maintain an excellent discharge machining state

under a high cutting current, a spiral discharge surface in the discharge channel, and a discharge characteristic with increased pulse interval; these attributes afford the stranded wire electrode a higher probability of effective discharge pulse compared to the normal wire electrode.

## 6 Conclusion

1. Although the effective discharge area of the stranded wire electrode was much smaller than that of the normal wire electrode in the processing direction at the same workpiece thickness, it has a higher probability of effective discharge pulse than the normal wire electrode under high energy and high thickness conditions because of its higher capacity of carrying liquid medium and removing debris, spiral discharge surface in the discharge channel, and discharge characteristic with increased pulse interval.
2. Due to the ample liquid medium in the electrode gap, the stranded wire electrode could withstand a higher average cutting current than the normal wire electrode. The experimental results show that the steady cutting speed of the stranded wire electrode was over 15,000 mm<sup>2</sup>/h (257 mm<sup>2</sup>/min) when the average cutting current was 18 A on a high-thickness workpiece.
3. The surface machined by the stranded wire electrode demonstrated better surface evenness than the normal wire electrode under conditions of high energy and high thickness.

**Acknowledgements** The authors extend their sincere thanks to those who contributed in the preparation of the instructions.

**Funding information** This project is supported by the National Natural Science Foundation of China (Grant No. 51575271 and No. 51675272).

**Publisher's Note** Springer Nature remains neutral with regard to jurisdictional claims in published maps and institutional affiliations.

## References

1. Maher I, Sarhan AAD, Hamdi M (2015) Review of improvements in wire electrode properties for longer working time and utilization in wire EDM machining. *Int J Adv Manuf Technol* 76:329–351. <https://doi.org/10.1007/s00170-014-6243-3>
2. Fan SY, Zhang QJ, Chen HW, Zeng WX (2013) Nonlinear dynamics analysis of multi-cutting wire electrode in WEDM-HS subjected to working fluid considering the effect of debris. *J Mech Sci Technol* 27:3595–3605
3. Haas P, Pontelandolfo P, Perez R (2013) Particle hydrodynamics of the electrical discharge machining process. Part 1: physical considerations and wire EDM process improvement. The seventeenth CIRP conference on electro physical and chemical machining (ISEM). *Procedia CIRP* 6:47–52
4. He XX, Liu ZD, Pan HW, Qiu MB, Zhang YQ (2017) Increasing process efficiency of HSWEDM based on discharge probability detection. *Int J Adv Manuf Technol* 93:3647–3654
5. Wang W, Liu ZD, Shi WT, Zhang YQ, Tian ZJ (2016) Surface burning of high-speed reciprocating wire electrical diacharge machining under large cutting energy. *Int J Adv Manuf Technol* 83: 2713–2720
6. Wan ZY (2008) Research on cutting technique in super-lager thickness WEDM [D]. Guangdong University of Technology 2008:2–5
7. Liu ZD (2014) The development trend of high speed reciprocating wire electrical discharge machining. *Machining Technology of Aeronautics* 19:40–45
8. Li MH, Bu FL (1996) Theoretical research on super-high thickness of WEDM [J]. *Journal of Shanghai Jiaotong University* 30(9):122–126
9. Liu ZD (2016) Development bottleneck and research strategy in reciprocating travelling WEDM [J]. *Electromachining Mould* 2016(S1):5–10
10. Xia LX (2015) Research on the discharge mechanism and the characteristic of compound dielectric fluid's life in HS-WEDM [D] Nanjing university of Aeronautics and Astronautics 2015: 1–2
11. Li CR, Liu ZD, Fang LJ, Pan HW, Qiu MB (2017) Super-high-thickness high-speed wire electrical discharge machining. *Int J Adv Manuf Technol* 2017:1–14
12. Zhang YQ, Liu ZD, Pan HW, Qiu MB (2017) Dielectric fluid lifespan detection based on pulse discharge probility in wire electrical discharge machining. *Int J Adv Manuf Technol* 92(1–4): 1481–1491. <https://doi.org/10.1007/s00170-017-0211-7>
13. Liu ZD, Chen HR, Pan HJ, Qiu MB, Tian ZJ (2014) Automatic control of WEDM servo for silicon processing using current pulse probability detection [J]. *Int J Adv Manuf Technol* 76(1–4):367–374
14. Pan HW, Liu ZD, Li CR (2017) Enhanced debris expelling in high-speed wire electrical discharge machining. *Int J Adv Manuf Technol* 93:2913–2292
15. Zhang Z, Huang H, Ming WY, Xu Z, Huang Y, Zhang GJ (2016) Study on machining characteristics of WEDM with ultrasonic vibration and magnetic field assisted techniques. *J Mater Process Technol* 234:342–352
16. Wang J, Han FZ (2014) Simulation model of debris and bubble movement in consecutive-pulse discharge of electrical discharge machining. *Int J Adv Manuf Technol* 74:591–598. <https://doi.org/10.1007/s00170-014-6008-z>